JCTC Journal of Chemical Theory and Computation

Properties and Permeability of Hypericin and Brominated Hypericin in Lipid Membranes

Emma S. E. Eriksson,[†,‡,||] Daniel J. V. A. dos Santos,[§] Rita C. Guedes,[§] and Leif A. Eriksson*[,†,||]

Örebro Life Science Center, School of Science and Technology, Örebro University, Fakultetsgatan 1, 70182 Örebro, Sweden, Modelling and Simulation Research Center, Örebro University, Örebro, Sweden, Department of Pharmacy, University of Lisbon, 1649-019 Lisbon, Portugal, and School of Chemistry, National University of Ireland, University Road, Galway, Ireland

Received May 25, 2009

Abstract: The promising photosensitizing properties of hypericin, a substituted phenanthroperylene quinone naturally found in Saint John's wort, has led to the proposal that it can be utilized in photodynamic therapy. Structurally modified derivatives are at the present time being investigated to generate a more effective hypericin photosensitizer. Neither the detailed mechanism behind the powerful action of hypericin, arising as a result of light excitation, nor the intracellular localization and transportation is still fully understood. In the present work, molecular dynamics simulations have been performed to study the properties and the permeability of hypericin and modifications thereof, substituted with one or four bromine atoms, in a dipalmitoylphosphatidylcholine lipid membrane. The molecules were found to accumulate in the most dense region of the lipids due to competing interactions with the hydrophobic lipid interior and the polar aqueous environment. This was confirmed by analyzing the radial distribution functions and by the density profiles of the system components. Calculated free energy profiles display large negative changes in free energy for the transport process of the molecules into the lipids, which also support this finding. Permeability coefficients show overall fastest diffusion in the membrane system for hypericin containing one bromine.

1. Introduction

1.1. Properties of Hypericin. Hypericin (Figure 1) is a phenanthroperylene quinone substituted with hydroxyl and alkyl groups that was first isolated from Saint John's wort (*Hypericum perforatum*) in 1911.[1] However, long before that, this plant was used in therapy as an antidepressant and in wound healing. More recently it has been shown that hypericin possesses toxicity against viruses such as hepatitis B[2], herpes,[3,4] and human immunodeficiency virus (HIV).[3,5−7] The molecule also displays antitumor activity, demonstrated both in vitro[8−10] and in vivo.[11−15] Both the antiviral and antitumor properties have been observed in the presence of light, and the chromophoric system along with the hydroxyl and alkyl substitution makes the molecule an efficient photosensitizer. This implies that the molecule might be used in photodynamic therapy (PDT), a three-component method in which a combination of light, administrated drug (a photosensitizer), and oxygen is required. PDT was first used in the 1970s and is now a promising treatment method of cancer and viral diseases. Tumors that are possible targets of this kind of therapy need to be more or less superficially located, either in the skin tissue or close beneath, to enable light penetration. Tumors located in cavities, such as the sinuses or stomach, are also treated using directed light.

* Corresponding author. E-mail: leif.eriksson@nuigalway.ie.
[†] Örebro Life Science Center, School of Science and Technology, Örebro University.
[‡] Modelling and Simulation Research Center; Örebro University.
[||] School of Chemistry, National University of Ireland.
[§] iMED.UL, CECF, Department of Pharmacy, University of Lisbon.

10.1021/ct9002702 CCC: $40.75
Published on Web 11/09/2009

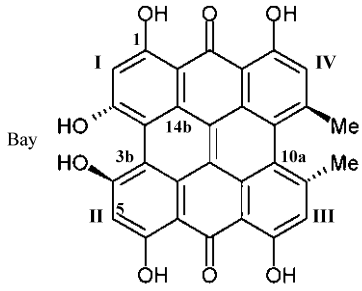

Figure 1. The hypericin molecule (Hy). The molecular axis is defined by the vector uniting carbon atoms 10a to 3b, and the molecular plane is defined by carbon atoms 10a, 3b, and 14b.[16] Bromine substitution was modeled at position I (Hy−Br) and positions I−IV (Hy−4Br).

Hypericin has a high ability to generate singlet oxygen and other reactive oxygen species (ROS) when irradiated by light. The quantum yield for singlet oxygen formation was at first estimated to be as high as 0.73,[17,18] but the number has later been revised to be as low as 0.36 in ethanol and to be less than 0.02 in water.[19] In liposomes, the quantum yields have been measured to be 0.35[20] and 0.43.[21] Given that these quantum yields are too low to explain the strong photodynamic action of the molecule, it can be concluded that there must be some additional mechanism involved.

Brominated hypericin at some of the positions (denoted with I−IV in Figure 1) are of considerable interest as they meet certain fundamental requirements for a photosensitizer. Brominated hypericins have displayed potential phototoxic activity, e.g., against the herpes simplex virus and the influenza virus.[22] It was also shown that some of these enhance the quantum yield of singlet oxygen and increase the quantum efficiency of superoxide formation compared with that of unsubstituted hypericin, as a result of enhanced intersystem crossing between the first excited singlet and triplet states.[23,24] A recent study from our group shows that one possible reaction of brominated hypericin after excitation is reduction followed by dissociation, generating a negatively charged bromine as a leaving group and a hypericin radical capable of binding to biological molecules.[25]

1.2. Transportation and Carriers of Hypericin. For drug molecules to reach possible cellular targets, they must transfer across the plasma membrane of the cell. The intracellular location and the way there, often mediated by the assistance of a carrier, depends on the properties of the molecules. This is an important field of study since the ROS generated from the photoreactions have short lifetimes and can only cause oxidative damage in the nearest surroundings. Several experimental studies suggest possible intracellular targets for photosentizisers, but for hypericin, the exact target and the transportation thereto are still not fully understood. One possible way for the molecule to enter the cell is through diffusion.[8] Another possible pathway to cellular transport is by accumulation in low-density lipoproteins (LDL)[15,26,27] and to a lower extent in high-density lipoproteins and human serum albumin[15,28−32] in human plasma when administrated into the bloodstream. Interaction with these biological molecules also helps to solubilize the highly hydrophobic hypericin molecule and to prevent aggregation, which otherwise would suppress virucidal activity and inhibit photodynamic properties. Another way to avoid aggregation and to solubilize the hypericin molecules is to encapsulate them into other appropriate drug-carriers, such as liposomes.[33] Tetra-brominated hypericin has been shown to exhibit higher binding constants to liposomes than hypericin as well as a higher singlet oxygen quantum yield compared to hypericin when bound to liposomes.[34]

1.3. Intracellular Location of Hypericin. The penetration of photosensitizers into various cell compartments, especially the nucleus, and their intracellular concentrations are important properties when considering cytotoxic activity. Although the exact intracellular location of hypericin is still unclear, the hydrophobic character of the molecule indicates accumulation in cytoplasmatic membranes, such as the endoplasmic reticulum and the Golgi apparatus, in which the molecule has also been found.[35−37]

Cholesterol carried by LDL is, upon entering the cell, directed to the lysosomes in which it is hydrolyzed. Hypericin encapsulated in LDL has been confirmed by several studies to end up located in the lysosomes.[38,39] Several model systems imply initial lysosomal damage caused by hypericin which triggers the mitochondrial apoptosis pathway.[40] Hypericin has been reported to accumulate in mitochondria,[38,41] and some pathways involve breakdown of the mitochondrial membrane.[42−44]

Studies also show an accumulation in the cell membrane.[8,45−47] One of these studies shows that only after long-term incubation, the molecules can penetrate the membrane and eventually reach the nucleus,[45] which has been pointed out as another possible target for hypericin.[45−47] Hypericin has been shown to interact with DNA, preferably with guanine and adenine nucleotide bases through formation of hydrogen bonds between position N7 of the purines and the hydroxyl groups of hypericin.[48−50]

Membrane lipid peroxidation can be another powerful consequence of photoinduced intracellular damage caused by hypericin.[51−53] Photosensitized hypericin has the ability to decrease the plasma membrane potential (depolarization) as well as the activity of Na^+, K^+-ATPase in liposome models;[53] which might have serious effects on the condition of a cell. Also in the treatment of various virus infections, membranes seem to be a potential target for hypericin, since only lipid-coated viruses are inactivated by the treatment.[54,55]

The widespread in findings of specific sites of intracellular localization of hypericin is probably due to the usage of different model systems, incubation time, and constitution of the incubation medium.

In order to obtain more insight on the action of hypericin in a biological environment, we here report the behavior of hypericin (Hy) with no, one (Hy−Br; position I, Figure 1) or four bromines (Hy−4Br; positions I−IV, Figure 1) inside a lipid dipalmitoylphosphatidylcholine (DPPC) bilayer, applying molecular dynamics simulations.

2. Theoretical Methodology

The molecular dynamics program GROMACS (version 3.3)[56,57] was used throughout the study. The membrane model used was an already equilibrated DPPC bilayer

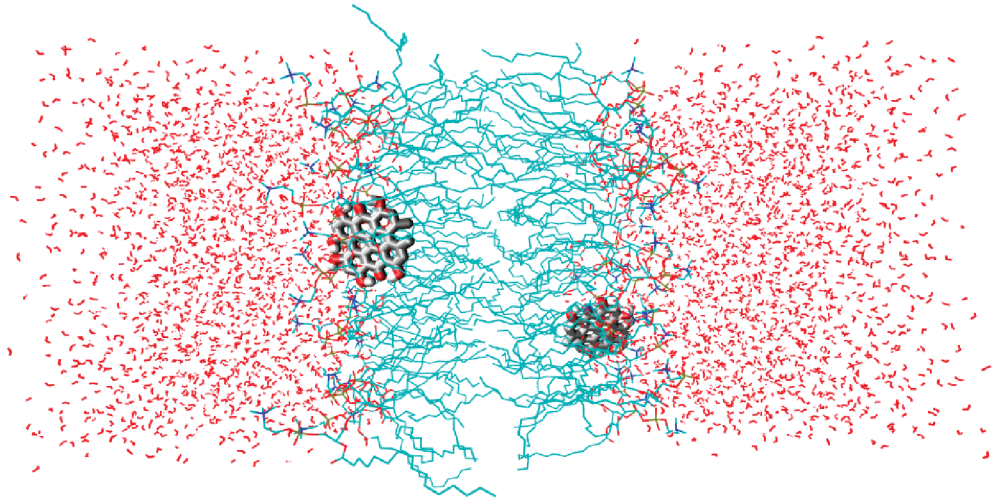

Figure 2. Snapshot from a simulation showing two hypericin molecules in a DPPC bilayer.

consisting of 64 lipids and 3 846 water molecules.[58,59] Three independent simulations were performed, one for each neutral hypericin derivative (Hy, Hy−Br, and Hy−4Br). The geometries of the hypericin molecules were generated from geometry optimizations of neutral hypericin derivatives in the quantum chemistry program Gaussian03[60] at the B3LYP/6-31G(d,p) level of theory. Mulliken atomic charges obtained from the geometry optimizations were assigned to the molecules. The GROMACS force field was used throughout. The topology of hypericin was obtained using the PRODRG software[61] through its web server (http://davapc1.bioch.dundee.ac.uk/prodrg/), using the PDB coordinates obtained in the quantum optimizations. As bromine is not parametrized in the force field, Lennard-Jones and ligand parameters for chlorine were used instead. For the DPPC phospholipids, a standard united-atom force field was applied,[62] and for water, we used the SPC model.[63] The starting point for each simulation was the resulting coordinates from previous 20 ns simulations using different conditions in which two hypericin molecules of each derivative were inserted into the membrane model, one in the outer region of the water phase and one in the middle of the lipid phase of the bilayer (this was part of an initial set of exploratory simulations to look for the general partition behavior of the molecules, and all the unconstrained equilibrium calculations were done using systems that contained the molecules already inside the lipid bilayer). These simulations resulted in both molecules locating in the lipid bilayer part of the system after a short equilibration, due to the hydrophobic character of the molecules. The systems were first equilibrated for 10 ns to uncorrelate those from the previous simulations, and followed by 50 ns productions in which the system trajectories were collected every 0.8 ps. During the simulations, none of the hypericin molecules moved out into the water phase or across the bilayer middle. The two molecules were located during the entire simulations in the lipid bilayer region, on opposite water/lipid interface sides, and were never close enough to interact strongly with each other (see Figure 2).

All simulations were performed using a time step of 2 fs and using the isothermal−isobaric ensemble at $T = 323$ K and $p = 1$ bar. The temperature and the pressure were held constant using a Nosé−Hoover thermostat[64,65] with a coupling constant of 0.1 ps and a semi-isotropic Parrinello−Rahman barostat[66,67] with a coupling constant of 1 ps. A particle mesh Ewald scheme[68,69] was used to calculate the electrostatic interactions with a 10 Å cutoff for the real space. The same cutoff was used for the short-range van der Waals interactions (Lennard-Jones terms). Bond lengths were constrained using the LINCS algorithm.[70]

Analysis was performed on the equilibration runs to check for equilibration convergence and on production runs from which all reported data was obtained. Data analysis programs written in C++ were used when no other program was available in the GROMACS package to calculate various properties reported herein.

A potential of mean force formalism was used to calculate free energy profiles for hypericin molecules across the lipid bilayer (the direction of the z-axis). The z-component of the force, F_z, acting on the molecule at certain constrained distances between the molecule and the bilayer center-of-mass was collected at different positions along the z-axis. The free energy for the transfer process between z_i and z_f is written as

$$\Delta G = G_{z_f} - G_{z_i} = -\int_{z_i}^{z_f} \langle F_z \rangle_z \mathrm{d}z \qquad (1)$$

where the bracket means an average over the forces collected at each constrained distance. To calculate the free energy profile for the translocation of each molecule, 41 constrained simulations were performed in which the hypericin molecule was located at different positions that differ by 0.1 Å along the z-axis direction. The starting points for the simulations were sampled from the previous unconstrained simulations. To sample the points in the middle of the bilayer, where the molecule was never located during the unconstrained simulations, a weak force was used to push the molecule toward the lipid bilayer, choosing the value of the force to make the least perturbation possible on the bilayer system. Each point in water was equilibrated for 1 ns, and a production run of 4 ns was used. Inside the lipid bilayer, an increase in the sampling was needed due to the slower motion of the molecules and, therefore, each point was equilibrated for at least 4.6 ns, and a production run of 10 ns followed. The force acting on the hypericin center-of-mass was

collected at every time step during the production run. A SHAKE algorithm[71] was used to constrain the distance between the center-of-mass of the bilayer and the hypericin molecules (the molecules were constrained in the z-direction but allowed to rotate).

The permeability is defined as the current density divided by the concentration gradient across the membrane. The procedure developed by Marrink and Berendsen[72] was adopted to calculate the permeability coefficients, based on the fluctuation dissipation theorem and on using the deviation of the instantaneous force, $F(z,t)$, from the average force acting on the molecule obtained during the constrained dynamics:

$$\Delta F(z,t) = F(z,t) - \langle F(z,t)\rangle \quad (2)$$

The local time-dependent friction coefficient, ξ, can be calculated from the following autocorrelation function:

$$\xi(z,t) = \langle \Delta F(z,t)\Delta F(z,0)\rangle / RT \quad (3)$$

where T is the absolute temperature and R is the gas constant. By integrating the friction coefficient, one can obtain the diffusion coefficient, D:

$$D(z) = RT/\xi(z) = (RT)^2 / \int_0^\infty \langle \Delta F(z,\mathrm{t})\Delta F(z,0)\rangle \mathrm{d}t \quad (4)$$

This function was fitted to a double exponential using a nonlinear fitting procedure[72] in order to integrate the autocorrelation of the force fluctuations:

$$C(t) = A_0 \exp(-t/\tau_0) + A_1 \exp(-t/\tau_1) \quad (5)$$

This illustrates that the molecules move inside the lipid bilayer in two distinct time scales, corresponding to the two decay times, τ_0 and τ_1, one fast and one slow.

The permeability coefficient, P, can be calculated by integrating over the local resistances across the membrane, $R(z)$. $R(z)$ is obtained by dividing the exponential of the previously calculated free energies, $\Delta G(z)$, by the diffusion coefficients, $D(z)$:

$$1/P = \int R(z)\mathrm{d}z = \int_{z_i}^{z_f} \frac{\exp(\Delta G(z)/kT)}{D(z)}\mathrm{d}z \quad (6)$$

3. Results and Discussion

Already during initial equilibration (unpublished data), the hypericin molecules moved into the lipids and remained there for the rest of the simulation. In Figure 2, we display a snapshot from the simulation. The probability of finding the molecules in the interface between the lipids and the water phase is high, as illustrated in Figure 3A for Hy−Br. In Figure 3B, the equilibrium distributions of all three hypericin derivatives are displayed. The figures show clearly that the probability to find the hypericin molecules is high close to the densest region of the membrane, i.e., close to the polar lipid head groups. The molecules are highly hydrophobic but also have some amphiphilic character due to the many hydroxyl groups. These groups have the ability to interact with water, which explains why such large and inflexible

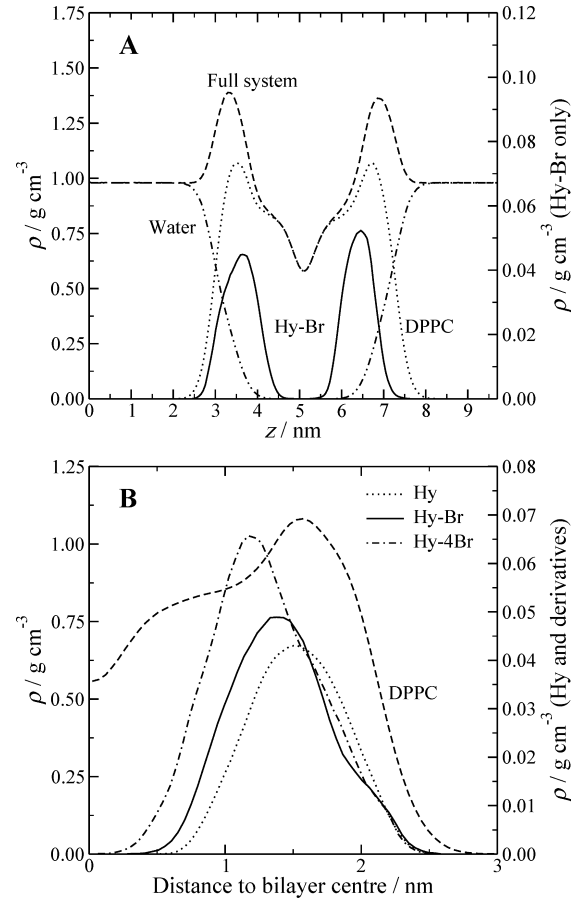

Figure 3. (A) Density profile for Hy−Br in the DPPC bilayer. (B) Resulting distribution for the three different hypericin derivatives as function of distance to the bilayer middle and compared with the DPPC density profile. The latter were obtained using the bilayer center-of-mass as the folding point.

molecules accumulate in the most dense region of the membrane, where they are within the lipid phase yet in contact with waters that penetrate into the bilayer. The final density profile of Hy−4Br is wider compared to Hy and Hy−Br, suggesting that this molecule is moving closer to the bilayer middle (the same applies to Hy−Br when compared to Hy). This affects the possibility to interact with surrounding water, as is discussed below in connection with radial distribution functions. Hypericin displays the most narrow density profile. None of the three molecules moves further out than 2.5 nm from the bilayer center. The density maximum is located closer to the bilayer center with an increasing level of bromination. A related study performed on the action of psoralen derivatives in lipid membranes showed similar accumulation in the lipid region, although slightly closer to the bilayer center (away from the densest region of the membrane), despite the smaller sizes of those compounds.[73] Generally similar partition profiles were also obtained for noncharged, hexyl ester and ethyl ester 5-aminolevulinic acids.[74]

A molecular axis tilt angle was defined as the vector uniting carbon 10a to carbon 3b (Figure 1), since those atoms belong to the inner and rigid part of the hypericin molecule and can give a clear idea about the orientation of the bay area of the molecule. An important aspect to account for is

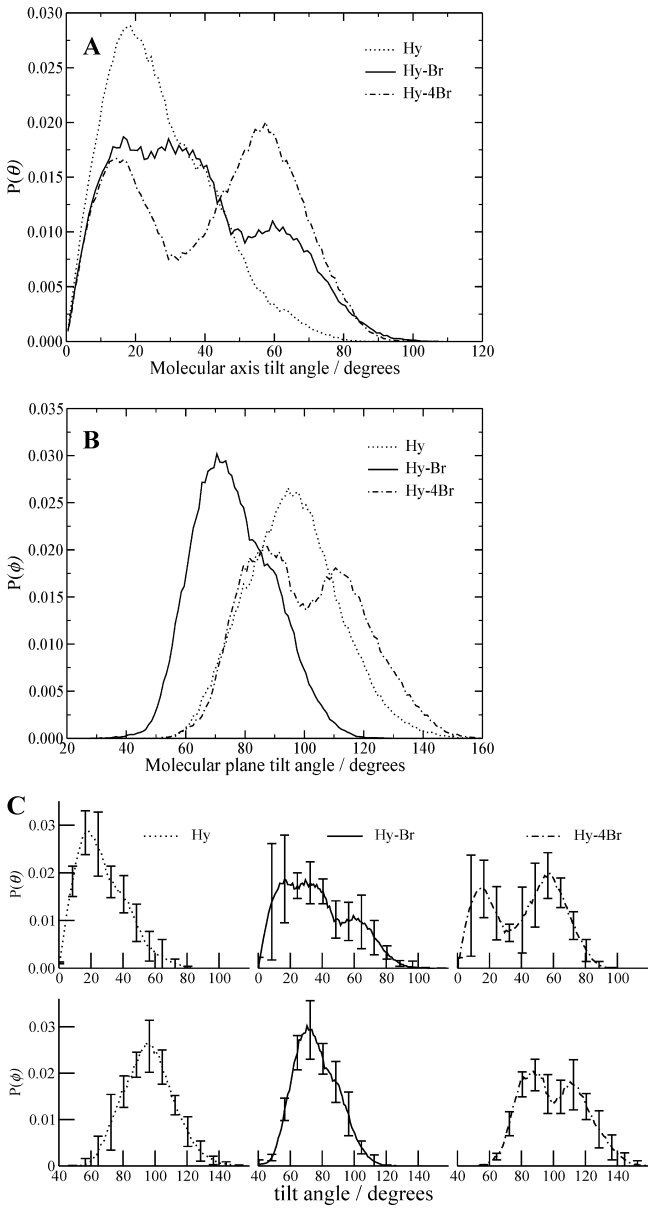

Figure 4. (A) The angle between the vector normal to the bilayer and the molecular axis vector pointing from atom C_{10a} to atom C_{3b}. (B) Molecular plane tilt angle, defined by the angle formed by the bilayer normal and the vector normal to the molecular plane. (C) Same plots as A and B for the molecular axis tilt (upper graphs) and molecular plane tilt (lower graphs) with the error bars this time displayed separately for clarity.

the fact that the bilayer is symmetric, with two interfaces between lipids and water, generating two normal vectors pointing in opposite directions. This was considered by subtracting normal vectors pointing toward negative values by 180°. The molecular axis tilt angle distributions for the hypericin derivatives are plotted in Figure 4A. The results are interpreted such that if the angle is 0° or 180°, then the molecular axis is parallel to the bilayer normal (the z-direction), and if the angle is 90°, then the molecular axis is perpendicular to the bilayer normal.

For hypericin, the distribution is much sharper than for the other two molecules and has a clear maximum located around 18°. For Hy−Br and Hy−4Br, the distributions are wider and bimodal, presenting two maxima, one located close to 16° (16−40° for Hy−Br) and another close to 58°. The major difference between the molecules is that an increased bromine content results in larger angle values, which are more probable. The first thing to note from these values is that the bay area of the molecule containing alcohol groups is oriented toward the water interface and the opposite part of the molecule containing the two methyl groups is located toward the inner and apolar part of the bilayer, in accordance with the hydrophobic nature of these.

A simple angle calculation shows that the molecules tend to maximize the interaction of the OH groups with the water interface. If the molecular axis tilt angle was 0°, then only two groups would be close to water, but by rotating ∼20°, the other two OH groups also surrounding the carbonyl oxygen are oriented closer to water. An angle of about 50° indicates that the bromine atoms become closer to water, and thus, in the molecules containing bromine atoms, there is a competitive balance between orienting both the OH and Br groups toward water. It is important to note that the probability to find an angle larger than or equal to 90° is essentially zero for all three molecules. This means that the methyl groups are never closer to the water interface than the OH groups.

The molecular plane was defined by carbons 10a, 3b, and 14b, and the plane tilt angle ϕ was defined by the angle formed by the bilayer normal and the vector normal to the molecular plane. The molecular plane tilt angle distributions for the hypericin derivatives are plotted in Figure 4B. The results are interpreted as follows: if the angle is 0° or 180°, then the molecular plane is aligned with the bilayer plane, and if the angle is 90°, then the molecular plane is perpendicular to the bilayer plane. Since hypericin and its derivatives have a disk-like shape, one would expect the molecule plane to be perpendicular to the bilayer plane, since this way less interfacial area is needed to fit each molecule inside the bilayer. This implies that plane tilt angles close to 0° or 180° would be difficult or impossible to find, but instead the plane tilt angle should be close to and somewhere around 90°. This is clearly seen in Figure 4B, where the tilt angle for all three molecules can vary between 40° to 150° with maxima close to 90°, especially for Hy and Hy−4Br.

The plane tilt angle maximum for Hy−Br is around 70°, that is, 20° off the molecule plane being perpendicular with the bilayer plane. For Hy we have a maximum around 95°, 5° away from an alignment with the perpendicular to the bilayer plane. For Hy−4Br we have a bimodal distribution, which means that the angles sampled preferentially around two maxima: one around ∼85° and another around ∼110°. Both maxima are centered around distributions of the same amplitude. One should take in consideration that, due to symmetry reasons, the relative position of the molecule is the same, if the plane tilt angle has the same divergence from 90°. This means that the first maximum of Hy−4Br (ϕ = 85°) has the same relative position in relation to the interface as Hy (ϕ = 95°). The other maximum of Hy−4Br, located close to 110°, has a deviation of 20° from being perpendicular to the bilayer plane, the same amount as for Hy−Br (ϕ = 70°). From these data, one can conclude that hypericin preferentially orients itself such that the molecular plane is

aligned along the z-axis of the bilayer. The addition of one bromine favors the molecular plane tilting, and with the addition of four bromine, the molecular symmetry is regained and the molecule orients in either position.

The error bars, considered as the standard deviation of the mean value:[75]

$$\sigma_{av} = \frac{\sigma}{\sqrt{(N/D - 1)}} \quad (7)$$

were calculated and are displayed in Figure 4C. Each error bar in the tilt distributions was calculated by dividing the production run in blocks of 1 ns ($N = 50$) and by calculating the standard deviation of the mean value of the blocks (σ). Autocorrelation functions (C_n) using these 50 values were used to calculate the decorrelation time D (time corresponding to C_n being equal to zero). With all this data, the error bars can be calculated according to the previous equation.

A simple test to see if the tilt axes distributions sample (or not) bimodal distributions is to split the 50 ns production runs in blocks and to analyze each block separately. If the tilt axis has a bimodal distribution, one can see in each block a clear preference in each molecule for one or the other bimodal zones and in between blocks the changing of probabilities of each bimodal zone because some molecule (or molecules) change the tilt and start to sample the other zone. The error bars also give an indication of this fact. For instance, the tilt molecular axis of the Hy−4Br molecule (Figure 4C, top right) can be found to preferentially sample values around 16° or 58°, and the error near 30° is lower because the two distributions have similar probabilities in that area. Moreover, the larger error bar for brominated hypericin is due to the fact that these molecules have the tendency to sample two different regions of the angle space, in opposition to hypericin that has only a single and sharp distribution.

Summarizing the molecular axis and molecular plane tilt angle distributions, we can conclude that hypericin and its derivatives are oriented in such a way to have the hydroxyl groups close to the water interface, with possible rotation to allow the bromine atoms to also become oriented toward this interface, and that the molecular plane is essentially perpendicular to the bilayer plane.

Radial distribution functions between oxygen atoms on the hypericin derivatives and hydrogen atoms in the surrounding water (Figure 5A) and between polar hydrogen atoms on the hypericin derivatives and oxygen atoms in the surrounding water (Figure 5B) were calculated. The first peak in both figures (at ∼0.18 nm) corresponds to a hydrogen bond. The following peak in Figure 5A corresponds to the second hydrogen in the same water molecule or a second solvation shell, whereas the second peak in Figure 5B corresponds to a second solvation shell of water. After this, there is an increase in amplitude of the radial distribution functions as more and more water molecules are included in the shells of higher order. The fact that hydrogen bonds are found implies that the molecules do interact with water. As the bay hydroxyl groups are located very close to the interface between the lipids and the water, these are the likely atoms/groups involved in hydrogen-bond formation. The

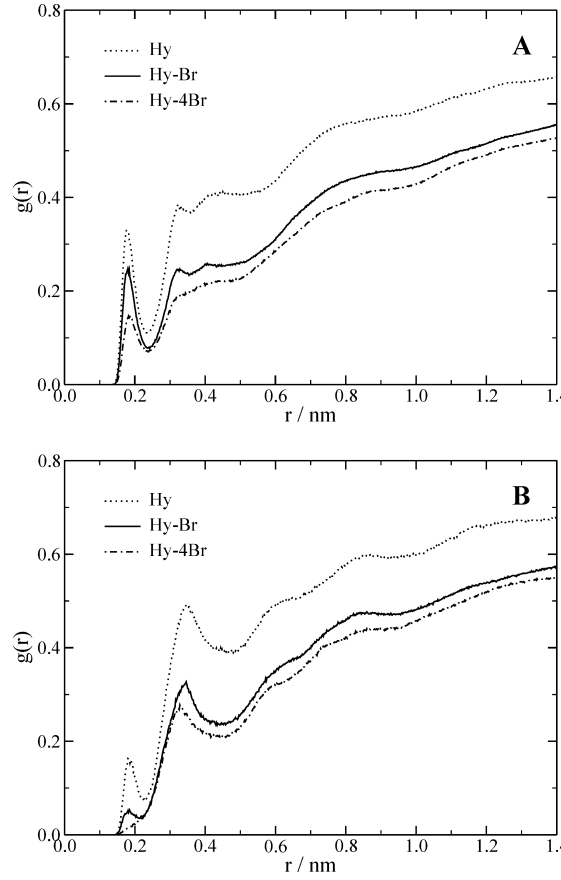

Figure 5. Radial distribution functions between (A) oxygen atoms on the hypericin derivatives and hydrogen atoms in the surrounding water; and (B) between polar hydrogen atoms on the hypericin derivatives and oxygen atoms in the surrounding water.

radial distribution functions decrease in the order Hy > Hy−Br > Hy−4Br, both in the case of hydrogen and oxygen interactions. The probability to find hydrogen bonds between oxygen on the hypericin molecules and hydrogen atoms in water is higher than between hypericin hydrogens and surrounding oxygen. This is due to the two lone pairs on oxygen that, hence, enables formation of two hydrogen bonds. Hydrogens bonds are detected for all molecules, involving hydrogen as well as oxygen on the hypericin molecules, except in the case involving hydrogen on Hy−4Br for which a peak is hardly visible. As discussed in connection with the density profiles above, Hy−4Br moves closer to the bilayer center compared to Hy and Hy−Br, which reduces the interaction with water and, thereby, results in lower radial distribution functions. Hypericin displays a more narrow density profile, positioned in the region closest to the interface between the lipids and water, and thus, the radial distribution functions are the highest for hypericin.

The mean-square displacement (MSD)[76] reveals details about the movements of the molecules inside the bilayer. The MSD is defined by

$$\mathrm{MSD}(t) = \langle |\vec{r}(t) - \vec{r}(0)|^2 \rangle \quad (8)$$

where $\vec{r}(0)$ and $\vec{r}(t)$ are the positions of a particle at time $t = 0$ and at a certain time t. The brackets indicate a time average

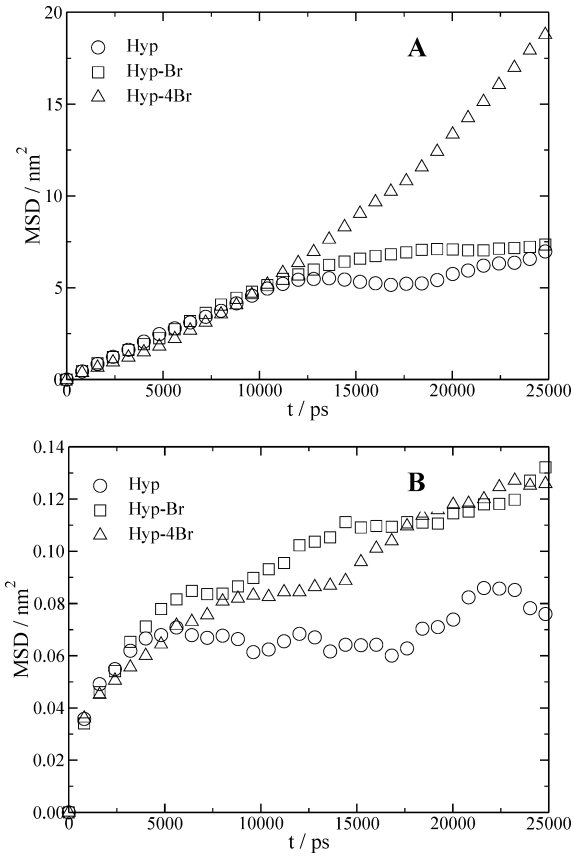

Figure 6. MSD in the (A) *xy*-plane and in the (B) direction normal to the bilayer.

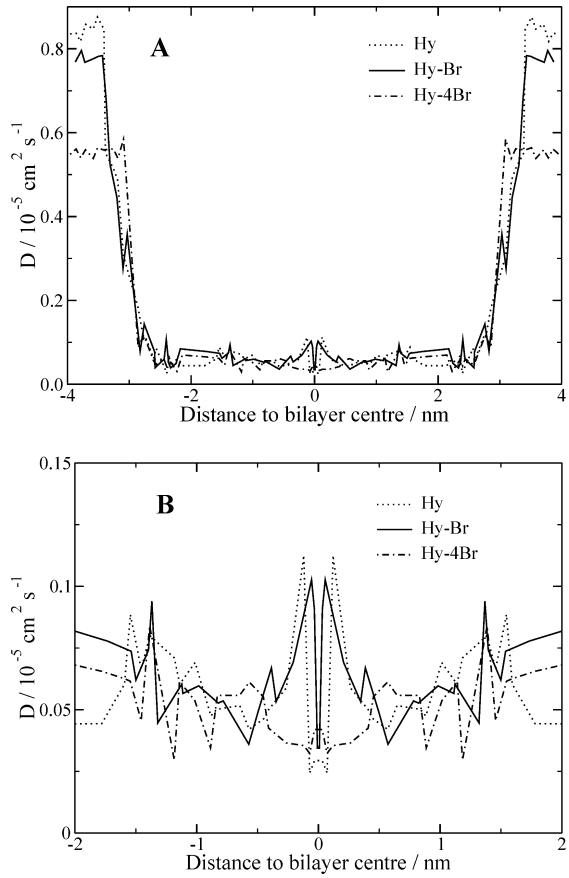

Figure 7. (A). Local diffusion coefficients of the hypericin derivatives in the DPPC bilayer, as functions of the distance to the bilayer middle. (B) Magnification of the region within 2 nm from the bilayer center.

over all similar particles and over different time origins along the simulation. The Einstein relation allows for the calculation of the diffusion coefficient, D, at sufficiently long simulation times:[76]

$$D = \lim_{t\to\infty} \frac{1}{2dt}\langle |r_i(t) - r_i(0)|^2 \rangle \qquad (9)$$

where d is the dimensionality of the space. This way, one can obtain the MSD for the molecules moving in the bilayer plane ($d = 2$) and moving along the bilayer normal ($d = 1$), respectively. The MSD provides a measure of the average distance a molecule travels in the system, and the growth rate of the MSD depends on how often the molecule collides, i.e., a measure of the ease of diffusion of the molecule.

Like other molecules diffusing in confined media, the hypericin molecules never reach the Einsteinian limit of proper diffusion within the limited time of the simulation, and anomalous diffusion occurs where MSD is proportional to t^n, with $0 < n < 1$.[77] The implication is that a direct comparison with experimental diffusion coefficients cannot be made. However, based on the MSD, one can state which molecules have a higher or a lower diffusive regime. The MSD in the bilayer plane and along the normal of the bilayer (z-direction) are displayed in Figure 6A and B, respectively. From Figure 6A, it is clear that the movement in the bilayer plane is not significantly changed by adding a bromine atom to hypericin, whereas the addition of four bromine atoms allows the molecule to move more easily. Although Hy−4Br is heavier, the MSD primarily reflects the hydrogen-bond capability, in accordance with the findings for the radial distribution functions that showed a clear decrease in hydrogen-bonding interaction between Hy−4Br and water.

One should be cautious in interpreting the MSD along the bilayer normal since this movement, as opposed to the movement in the bilayer plane, is finite, and hence, the MSD should level off independently of any characteristic of the molecule under consideration. Anyway this property is displayed in Figure 6B and shows that the addition of at least one bromine atom increases the diffusion of the molecules. This again shows that the higher ability of hypericin to form hydrogen bonds with water makes its average position closer to the lipid−water interface (i.e., the time spent at the interface is larger) and hinders both the movement of the molecule in the direction normal to the bilayer and in the bilayer plane. Comparing both movements in the bilayer, it is also clear that the diffusion in the bilayer plane is much higher than that in the z-direction, for all molecules.

The local diffusion coefficients across the bilayer were calculated by integrating the fitted autocorrelation functions (eq 4), and the dependence on the distance to the bilayer center is displayed in Figure 7A and B (the latter showing only the region within 2 nm from the bilayer center). Figure 7A shows a significant difference between the diffusion coefficients in the lipid region of the bilayer and in the water phase. The diffusion of the molecules in water is faster than

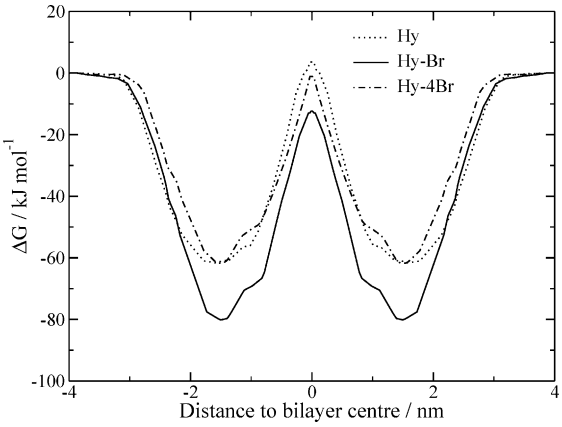

Figure 8. Free energy profiles for the hypericin derivatives inside the DPPC bilayer.

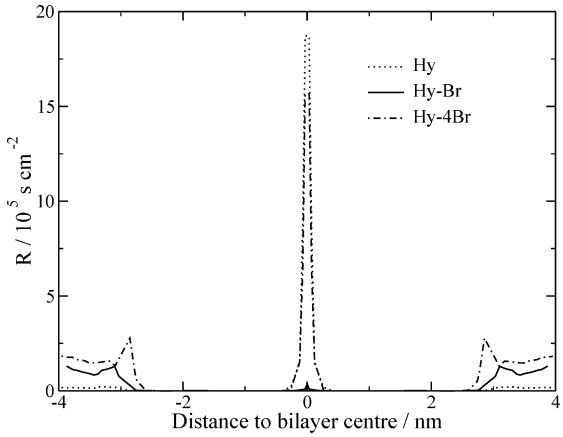

Figure 9. Local resistance profiles of the different hypericin derivatives in the DPPC bilayer, as functions of the distance to the bilayer middle. The hypericin profile was scaled down by a factor 7.

Table 1. Permeability Coefficients Inside the DPPC Bilayer (cm s^{-1})

molecule	permeability coefficients
Hy	4.21×10^{-4}
Hy−Br	4.94×10^{-3}
Hy−4Br	1.51×10^{-3}

inside the lipids, since the water molecules can rearrange faster around the hypericin molecules as they move around. When hypericin is inside the bilayer, space must be created by the much slower moving lipid molecules before it can move to another position. Inside water, the diffusion coefficients of the molecules decrease with increased bromine content. This seems to be caused by the different molecular size and especially by the different molecular weights of the molecules, where the heavier and the larger molecule moves more slowly.

Looking closer at the diffusion coefficients within the lipid region of the bilayer (Figure 7B), it can be seen that Hy−4Br moves slower than the other two molecules, also in the very middle of the bilayer where the density is at its lowest. The other two molecules show a minor increase in diffusion very close to the bilayer center, with very similar profiles.

Free energy profiles for the transport process from water and into the lipids, as functions of the distance to the bilayer center, were calculated using the potential of mean force formalism outlined above (Figure 8).[78] In similar calculations, using the same technique but only 2 ns in the production runs (we used 4 ns in water and 10 ns in the lipid bilayer),[79] they obtained errors in the free energy that ranged from about 0.7 to 4 kJ/mol in the bilayer middle, where the errors were found to be larger and, in a way, that was not clearly dependent on the size of the molecules studied. The profiles show a local minimum in the region 1−2 nm from the bilayer center, near the polar headgroup region, when moving from the water phase into the lipids. Having passed this minimum, the free energy increases when the molecules move toward the bilayer middle. Hy is the only one of the three molecules which shows a positive change in free energy at the very middle of the bilayer, with an increase of ∼3.5 kJ/mol compared to furthest out in the water phase. Hy−4Br shows a decrease of ∼1.2 kJ/mol, and Hy-Br shows a decrease of ∼12.3 kJ/mol in the bilayer middle. Hy−Br also displays a deeper free energy minimum, ∼18 kJ/mol lower than for Hy and Hy−4Br, in the region close to the polar headgroups. This indicates that Hy−Br is the most likely to accumulate inside the lipids, and, since the diffusion in the lipid region is low, the molecules are more likely to reside in the polar headgroup region of the bilayer.

From the calculated free energy profiles and the local diffusion coefficients across the lipid bilayer, the local resistance was calculated using eq 6, and the resulting profiles for the three molecules are displayed in Figure 9. To display all three molecules more clearly, the Hy resistance profile was scaled down by a factor 7. For all three molecules, an increase in resistance was found in the bilayer middle, although for Hy−Br this is much less than for Hy and Hy−4Br. For Hy and Hy−4Br, the peaks in the center are considerably higher than the increased resistance seen in the water phase, whereas for Hy−Br the opposite is noted. The free energy plays a dominant role in the appearance of the resistance profiles, and the increase in free energy in the middle of the bilayer is in accordance with the increased resistance in this region.

Permeability coefficients were calculated by integrating the resistance profiles across the bilayer, and from those, it can be concluded that the permeation decreases in the order Hy−Br > Hy−4Br > Hy (Table 1). As mentioned before, the permeability strongly depends on the free energy, and the decrease in permeation follows the increase in energy. Hy−Br displays a significantly lower free energy, both close to the polar headgroups of the lipids and in the center of the lipids, than the other two which contributes to an easier and, therefore, faster permeation. An experimental study has shown that halogenation of drug molecules enhances permeation by increasing the permeability coefficients and enhances the free energy of transfer into the lipid membrane, as compared to the nonsubstituted molecules.[80] Those results are in agreement with our findings that the brominated hypericins display higher permeability coefficients than that of the nonsubstituted hypericin.

Estimated permeability coefficients from experiments of hypericin across monolayers of Caco-2 cells are in the order

of 10^2-10^3 less than those calculated herein.[46] The difference when comparing experimental and calculated permeability coefficients is probably due to that natural membranes contain many more components, such as proteins and cholesterol, which can either enhance or suppress the permeability through the membrane. The present computational study was performed with a simplified membrane model and with the aim to study passive permeation only, and how the permeability is affected by different levels of bromination.

Conclusions

Three hypericin derivatives were studied in order to reveal their distribution and specific properties in a DPPC lipid membrane, using classical molecular dynamics simulations. All three molecules showed a strong preference to accumulate in the densest region of the membrane, close to the polar headgroups. Hypericin accumulates closest to the interface between the lipids and water. This is also manifested by radial distribution functions which show the highest number of hydrogen bonds between hypericin and water. Local diffusion coefficients show, as expected, high-diffusion rates in the water phase compared to that of the lipids, due to the large size and hydrophobic character of the molecules. Calculated permeability coefficients suggest a faster overall diffusion for Hy−Br. This finding is also supported by the free energy profiles which displays a more negative change in free energy for the transport process of Hy−Br moving from water into the lipids. For all three hypericin derivatives, the free energy profiles display minima within 1−2 nm from the bilayer center, in the same region as where the molecules were found to accumulate according to the density profiles. According to the present results, we can expect more of Hy and Hy−4Br to accumulate within the membrane, suggesting a larger possibility of direct photodamage caused by those. Hy−Br has a higher capability to translocate across the membrane and would potentially have a larger probability to penetrate the membrane and, thus, reach other targets in the interior of a cell.

Acknowledgment. Financial support from the Modelling and Simulation Research Center (ESEE), the Swedish Research Council, the Faculty of Science and Technology at Örebro University, and the National University of Ireland, Galway (LAE), is gratefully acknowledged. We also acknowledge generous grants of computing time at the National Supercomputing Center (NSC) in Linköping. The Portuguese Fundação para a Ciência e a Tecnologia is also acknowledged for financial support.

References

(1) Cerny, C. *Z. Phys. Chem.* **1911**, *73*, 371–382.

(2) Moraleda, G.; Wu, T. T.; Jilbert, A. R.; Aldrich, C. E.; Condreay, L. D.; Larsen, S. H.; Tang, J. C.; Colacino, J. M.; Mason, W. S. *Antivir. Res.* **1993**, *20*, 235–247.

(3) Lopezbazzocchi, I.; Hudson, J. B.; Towers, G. H. N. *Photochem. Photobiol. Sci.* **1991**, *54*, 95–98.

(4) Hudson, J. B.; Lopezbazzocchi, I.; Towers, G. H. N. *Antivir. Res.* **1991**, *15*, 101–112.

(5) Meruelo, D.; Lavie, G.; Lavie, D. *Proc. Natl. Acad. Sci. U.S.A.* **1988**, *85*, 5230–5234.

(6) Lenard, J.; Rabson, A.; Vanderoef, R. *Proc. Natl. Acad. Sci. U.S.A.* **1993**, *90*, 158–162.

(7) Degar, S.; Prince, A. M.; Pascual, D.; Lavie, G.; Levin, B.; Mazur, Y.; Lavie, D.; Ehrlich, L. S.; Carter, C.; Meruelo, D. *AIDS Res. Hum. Retroviruses* **1992**, *8*, 1929–1936.

(8) Thomas, C.; Pardini, R. S. *Photochem. Photobiol. Sci.* **1992**, *55*, 831–837.

(9) Andreoni, A.; Colasanti, A.; Colasanti, P.; Mastrocinque, M.; Riccio, P.; Roberti, G. *Photochem. Photobiol. Sci.* **1994**, *59*, 529–533.

(10) VanderWerf, Q. M.; Saxton, R. E.; Chang, A.; Horton, D.; Paiva, M. B.; Anderson, J.; Foote, C.; Soudant, J.; Mathey, A.; Castro, D. J. *Laryngoscope* **1996**, *106*, 479–483.

(11) Thomas, C.; Pardini, L.; Pardini, R. S. In 3rd Biennial Meeting of the International Photodynamic Association; Buffalo, NY, 1990.

(12) Chung, P. S.; Rhee, C. K.; Kim, K. H.; Paek, W.; Chung, J.; Paiva, M. B.; Eshraghi, A. A.; Castro, D. J.; Saxton, R. E. *Laryngoscope* **2000**, *110*, 1312–1316.

(13) Liu, C. D.; Kwan, D.; Saxton, R. E.; McFadden, D. W. *J. Surg. Res.* **2000**, *93*, 137–143.

(14) Chen, B.; de Witte, P. A. *Cancer Lett.* **2000**, *150*, 111–117.

(15) Chen, B.; Xu, Y.; Roskams, T.; Delaey, E.; Agostinis, P.; Vandenheede, J. R.; de Witte, P. *Int. J. Cancer* **2001**, *93*, 275–282.

(16) Freeman, D.; Konstantinovskii, L.; Mazur, Y. *Photochem. Photobiol. Sci.* **2001**, *74*, 206–210.

(17) Jardon, P.; Lazortchak, N.; Gautron, R. *J. Chim. Phys. Phys.-Chim. Biol.* **1987**, *84*, 1141–1145.

(18) Racinet, H.; Jardon, P.; Gautron, R. *J. Chim. Phys. Phys.-Chim. Biol.* **1988**, *85*, 971–977.

(19) Darmanyan, A. P.; Burel, L.; Eloy, D.; Jardon, P. *J. Chim. Phys. Phys.-Chim. Biol.* **1994**, *91*, 1774–1785.

(20) Bouirig, H.; Eloy, D.; Jardon, P. *J. Chim. Phys. Phys.-Chim. Biol.* **1992**, *89*, 1391–1411.

(21) Ehrenberg, B.; Anderson, J. L.; Foote, C. S. *Photochem. Photobiol. Sci.* **1998**, *68*, 135–140.

(22) Hudson, J. B.; Delaey, E.; De Witte, P. A. *Photochem. Photobiol. Sci.* **1999**, *70*, 820–822.

(23) Delaey, E.; Zupko, I.; Chen, B.; Derycke, A.; Van Laar, F.; De Vos, D.; De Witte, P. *Int. J. Oncol.* **2003**, *23*, 519–524.

(24) Guedes, R. C.; Eriksson, L. A. *J. Photochem. Photobiol., A* **2006**, *178*, 41–49.

(25) Eriksson, E. S. E.; Guedes, R. C.; Eriksson, L. A. *Int. J. Quantum Chem.* **2008**, *108*, 1921–1929.

(26) Kascakova, S.; Refregiers, M.; Jancura, D.; Sureau, F.; Maurizot, J. C.; Miskovsky, P. *Photochem. Photobiol. Sci.* **2005**, *81*, 1395–1403.

(27) Mukheriee, P.; Adhikary, R.; Halder, M.; Petrich, J. W.; Miskovsky, P. *Photochem. Photobiol. Sci.* **2008**, *84*, 706–712.

(28) Sjoholm, I.; Ekman, B.; Kober, A.; Ljungstedtpahlman, I.; Seiving, B.; Sjodin, T. *Mol. Pharmacol.* **1979**, *16*, 767–777.

(29) Falk, H.; Meyer, J. *Monatsh. Chem.* **1994**, *125*, 753–762.

(30) Kohler, M.; Gafert, J.; Friedrich, J.; Falk, H.; Meyer, J. *J. Phys. Chem.* **1996**, *100*, 8567–8572.

(31) Miskovsky, P.; Jancura, D.; Sanchez-Cortes, S.; Kocisova, E.; Chinsky, L. *J. Am. Chem. Soc.* **1998**, *120*, 6374–6379.

(32) Miskovsky, P.; Hritz, J.; Sanchez-Cortes, S.; Fabriciova, F.; Ulicny, J.; Chinsky, L. *Photochem. Photobiol. Sci.* **2001**, *74*, 172–183.

(33) Vemuri, S.; Rhodes, C. T. *Pharm. Acta Helv.* **1995**, *70*, 95–111.

(34) Roslaniec, M.; Weitman, H.; Freeman, D.; Mazur, Y.; Ehrenberg, B. *J. Photochem. Photobiol., B* **2000**, *57*, 149–158.

(35) Vandenbogaerde, A. L.; Delaey, E. M.; Vantieghem, A. M.; Himpens, B. E.; Merlevede, W. J.; de Witte, P. A. *Photochem. Photobiol. Sci.* **1998**, *67*, 119–125.

(36) Uzdensky, A. B.; Ma, L. W.; Iani, V.; Hjortland, G. O.; Steen, H. B.; Moan, J. *Laser Med. Sci.* **2001**, *16*, 276–283.

(37) Delaey, E. M.; Obermueller, R.; Zupko, I.; De Vos, D.; Falk, H.; de Witte, P. A. M. *Photochem. Photobiol. Sci.* **2001**, *74*, 164–171.

(38) Ali, S. M.; Chee, S. K.; Yuen, G. Y.; Olivo, M. *Int. J. Mol. Med.* **2002**, *9*, 257–270.

(39) Siboni, G.; Weitman, H.; Freeman, D.; Mazur, Y.; Malik, Z.; Ehrenberg, B. *Photochem. Photobiol. Sci.* **2002**, *1*, 483–491.

(40) Guicciardi, M. E.; Leist, M.; Gores, G. J. *Oncogene* **2004**, *23*, 2881–2890.

(41) Theodossiou, T. A.; Noronha-Dutra, A.; Hothersall, J. S. *Int. J. Biochem. Cell Biol.* **2006**, *38*, 1946–1956.

(42) Vantieghem, A.; Assefa, Z.; Vandenabeele, P.; Declercq, W.; Courtois, S.; Vandenheede, J. R.; Merlevede, W.; de Witte, P.; Agostinis, P. *FEBS Lett.* **1998**, *440*, 19–24.

(43) Vantieghem, A.; Xu, Y.; Vandenabeele, P.; Denecker, G.; Vandenheede, J. R.; Merlevede, W.; de Witte, P. A.; Agostinis, P. *Photochem. Photobiol. Sci.* **2001**, *74*, 133–142.

(44) Berlanda, J.; Kiesslich, T.; Oberdanner, C. B.; Obermair, F. J.; Krammer, B.; Plaetzer, K. *J. Environ. Pathol. Toxicol. Oncol.* **2006**, *25*, 173–188.

(45) Miskovsky, P.; Sureau, F.; Chinsky, L.; Turpin, P. Y. *Photochem. Photobiol. Sci.* **1995**, *62*, 546–549.

(46) Sattler, S.; Schaefer, U.; Schneider, W.; Hoelzl, J.; Lehr, C. M. *J. Pharm. Sci.* **1997**, *86*, 1120–1126.

(47) English, D. S.; Doyle, R. T.; Petrich, J. W.; Haydon, P. G. *Photochem. Photobiol. Sci.* **1999**, *69*, 301–305.

(48) Miskovsky, P.; Chinsky, L.; Wheeler, G. V.; Turpin, P. Y. *J. Biomol. Struct. Dyn.* **1995**, *13*, 547–552.

(49) SanchezCortes, S.; Miskovsky, P.; Jancura, D.; Bertoluzza, A. *J. Phys. Chem.* **1996**, *100*, 1938–1944.

(50) Kocisova, E.; Chinsky, L.; Miskovsky, P. *J. Biomol. Struct. Dyn.* **1998**, *15*, 1147–1154.

(51) Senthil, V.; Jones, L. R.; Senthil, K.; Grossweiner, L. I. *Photochem. Photobiol. Sci.* **1994**, *59*, 40–47.

(52) Hadjur, C.; Richard, M. J.; Parat, M. O.; Jardon, P.; Favier, A. *Photochem. Photobiol. Sci.* **1996**, *64*, 375–381.

(53) Chaloupka, R.; Obsil, T.; Plasek, J.; Sureau, F. *Biochim. Biophys. Acta Biomembr.* **1999**, *1418*, 39–47.

(54) Tang, J.; Colacino, J. M.; Larsen, S. H.; Spitzer, W. *Antivir. Res.* **1990**, *13*, 313–325.

(55) Hudson, J. B.; Towers, G. H. N. *Pharmacol. Therapeut.* **1991**, *49*, 181–222.

(56) Lindahl, E.; Hess, B.; van der Spoel, D. *J. Mol. Model.* **2001**, *7*, 306–317.

(57) Van der Spoel, D.; Lindahl, E.; Hess, B.; Groenhof, G.; Mark, A. E.; Berendsen, H. J. C. *J. Comput. Chem.* **2005**, *26*, 1701–1718.

(58) Marrink, S. J.; Berger, O.; Tieleman, P.; Jahnig, F. *Biophys. J.* **1998**, *74*, 931–943.

(59) Biocomputing at the University of Calgary, Structures and Topologies. http://moose.bio.ucalgary.ca/index.php?page=Structures_and_Topologies. Accessed December 1, 2007), File: dppc64.pdb.

(60) Frisch, M. J.; Trucks, G. W.; Schlegel, H. B.; Scuseria, G. E.; Robb, M. A.; Cheeseman, J. R.; Jr., J. A. M.; Vreven, T.; Kudin, K. N.; Burant, J. C.; Millam, J. M.; Iyengar, S. S.; Tomasi, J.; Barone, V.; Mennucci, B.; Cossi, M.; Scalmani, G.; Rega, N.; Petersson, G. A.; Nakatsuji, H.; Hada, M.; Ehara, M.; Toyota, K.; Fukuda, R.; Hasegawa, J.; Ishida, M.; Nakajima, T.; Honda, Y.; Kitao, O.; Nakai, H.; Klene, M.; Li, X.; Knox, J. E.; Hratchian, H. P.; Cross, J. B.; Adamo, C.; Jaramillo, J.; Gomperts, R.; Stratmann, R. E.; Yazyev, O.; Austin, A. J.; Cammi, R.; Pomelli, C.; Ochterski, J. W.; Ayala, P. Y.; Morokuma, K.; Voth, G. A.; Salvador, P.; Dannenberg, J. J.; Zakrzewski, V. G.; Dapprich, S.; Daniels, A. D.; Strain, M. C.; Farkas, O.; Malick, D. K.; Rabuck, A. D.; Raghavachari, K.; Foresman, J. B.; Ortiz, J. V.; Cui, Q.; Baboul, A. G.; Clifford, S.; Cioslowski, J.; Stefanov,B. B.; Liu, G.; Liashenko, A.; Piskorz, P.; Komaromi, I.; Martin, R. L.; Fox, D. J.; Keith, T.; Al-Laham, M. A.; Peng, C. Y.; Nanayakkara, A.; Challacombe, M.; Gill, P. M. W.; Johnson, B.; Chen, W.; Wong, M. W.; Gonzalez, C.; Pople, J. A. *Gaussian03; Rev E.01*; Gaussian, Inc.: Pittsburgh PA, 2003.

(61) Schuttelkopf, A. W.; van Aalten, D. M. *Acta Crystallogr., Sect. D: Biol. Crystallogr.* **2004**, *60*, 1355–63.

(62) Biocomputing at the University of Calgary, Structures and Topologies. http://moose.bio.ucalgary.ca/index.php?page=Structures_and_Topologies. Accessed December 1, 2007), Files: lipid.itp and dppc.itp.

(63) Berendsen, H. J. C.; Postma, J. P. M.; van Gunsteren, W. F.; Hermans, J. In *Intermolecular Forces*; Pullman, B., Ed.; Reidel Publishing Company: Dordrecht, Netherlands, 1981.

(64) Nose, S. *Mol. Phys.* **1984**, *52*, 255–268.

(65) Hoover, W. G. *Phys. Rev.* **1985**, *31*, 1695–1697.

(66) Parrinello, M.; Rahman, A. *J. Appl. Phys.* **1981**, *52*, 7182–7190.

(67) Nose, S.; Klein, M. L. *Phys. Rev. Lett.* **1983**, *50*, 1207–1210.

(68) Darden, T.; York, D.; Pedersen, L. *J. Chem. Phys.* **1993**, *98*, 10089–10092.

(69) Essmann, U.; Perera, L.; Berkowitz, M. L.; Darden, T.; Lee, H.; Pedersen, L. G. *J. Chem. Phys.* **1995**, *103*, 8577–8593.

(70) Hess, B.; Bekker, H.; Berendsen, H. J. C.; Fraaije, J. *J. Comput. Chem.* **1997**, *18*, 1463–1472.

(71) Ryckaert, J. P.; Ciccotti, G.; Berendsen, H. J. C. *J. Comput. Phys.* **1977**, *23*, 327–341.

(72) Marrink, S. J.; Berendsen, H. J. C. *J. Phys. Chem.* **1994**, *98*, 4155–4168.

(73) dos Santos, D. J. V. A.; Eriksson, L. A. *Biophys. J.* **2006**, *91*, 2464–2474.

(74) Erdtman, E.; dos Santos, D. J. V. A.; Lofgren, L.; Eriksson, L. A. *Chem. Phys. Lett.* **2008**, *463*, 178–182.

(75) dos Santos, D. J. V. A.; Muller-Plathe, F.; Weiss, V. C. *J. Phys. Chem. C* **2008**, *112*, 19431–19442.

(76) Allen, M. P.; Tildesley, D. J. *Computer Simulation of Liquids*; Oxford University Press: Oxford, U.K., 1990.

(77) Müller-Plathe, F.; Rogers, S. C.; van Gunsteren, W. F. *Chem. Phys. Lett.* **1992**, *199*, 237–243.

(78) Paci, E.; Ciccotti, G.; Ferrario, M.; Kapral, R. *Chem. Phys. Lett.* **1991**, *176*, 581–587.

(79) Bemporad, D.; Essex, J. W.; Luttmann, C. *J. Phys. Chem. B* **2004**, *108*, 4875–4884.

(80) Gerebtzoff, G.; Li-Blatter, X.; Fischer, H.; Frentzel, A.; Seelig, A. *ChemBioChem* **2004**, *5*, 676–684.

CT9002702